Waveform similarity analysis using graph mining for the optimization of sensor positioning in wearable seismocardiography

Francesca Santucci, *Student Member, IEEE*, Martina Nobili, Daniela Lo Presti, *Associate Member, IEEE*, Carlo Massaroni, *Senior Member, IEEE*, Roberto Setola, *Senior Member, IEEE*, Emiliano Schena, *Senior Member, IEEE* and Gabriele Oliva, *Senior Member, IEEE*

***Abstract*— Objective: A major concern with wearable devices aiming to measure the seismocardiogram (SCG) signal is the variability of SCG waveform with the sensor position and a lack of a standard measurement procedure. We propose a method to optimize sensor positioning based on the similarity among waveforms collected through repeated measurements. Method: we design a graph-theoretical model to evaluate the similarity of SCG signals and apply the proposed methodology to signals collected by sensors placed in different positions on the chest. A *similarity score* returns the optimal measurement position based on the repeatability of SCG waveforms. We tested the methodology on signals collected by using two wearable patches based on optical technology placed in two positions: mitral and aortic valve auscultation site (inter-position analysis). 11 healthy subjects were enrolled in this study. Moreover, we evaluated the influence of the subject's posture on waveform similarity with a view on ambulatory use (inter-posture analysis). Results: the highest similarity among SCG waveforms is obtained with the sensor on the mitral valve and the subject laying down. Conclusions: our approach aims to be a step forward in the optimization of sensor positioning in the field of wearable seismocardiography. We demonstrate that the proposed algorithm is an effective method to estimate similarity among waveforms and outperforms the state-of-the-art in comparing SCG measurement sites. Significance: results obtained from this study can be exploited to design more efficient protocols for SCG recording in both research studies and future clinical examinations.**

***Index Terms*— seismocardiogram (SCG), SCG waveform, wearables, fiber optic sensors, graph theory, cardiovascular monitoring**

I. Introduction

Seismocardiography has proven to be a promising tool for a non-invasive monitoring of cardiac mechanics. Compared to traditional methods, e.g., electrocardiogram (ECG) and photoplethysmogram (PPG), this technique has the potential of providing direct information on hemodynamic parameters, cardiac time intervals and mechanical events related to the cardiac cycle [1]–[3]. This is particularly important for future clinical use [4]–[6]. Seismocardiogram (SCG) essentially amounts to a signal that measures minute thorax vibrations produced by the beating heart on the chest wall surface [7], [8]. This signal can be recorded in different modalities, which include contact and contactless measurement methods. Contactless techniques include laser doppler vibrometers, microwave doppler radars, and airborne ultrasound surface motion camera [9]. For what concerns contact-based methods, these microscopic vibrations can be recorded in the form of accelerations, angular velocities or deformations using accelerometers, gyroscopes or Fiber Bragg Grating (FBGs) sensors, respectively [10]. FBGs, being immune to electromagnetic interferences, broaden the clinical application scenarios of seismocardiography. For instance, they are allowed to be used in harsh environments like Magnetic Resonance room, where their electrical counterparts are forbidden. Contact-based methods are catching on fast with the growing popularity of wearable devices, that allow a prolonged and remote monitoring of cardiac function with the lowest discomfort for the patient. A critical concern in wearable seismocardiography is the lack of a global standard for sensor positioning. Indeed, SCG waveform is characterized by a variability that depends on different factors, including sensor positioning. The measurement areas investigated in the literature change slightly depending on the type of sensor unit embedded in the wearable device and on the overall design and dimensions of the system [10]. To date, the most investigated positions are the mitral valve, the 4 valves auscultation sites, the space between the second and third rib, the middle of the sternum, and the left lower border of the sternum [9].

In the literature, very few attempts have been made to assess the optimal position on the chest for SCG recording [11], [12]. For instance, Lo Presti et. al. investigated the accuracy in heart rate (HR) estimation of an FBG-based wearable with respect to 3 different positions on the chest [12]. In this study, the most promising position for SCG recording on the basis of HR estimation resulted to be the mitral valve. However, the literature is lacking in definitive studies

F. Santucci, M. Nobili, G. Oliva, and R. Setola are with the Unit of Automatic Control, Universitá Campus Bio-Medico di Roma, Rome, RM 00128 Italy. (e-mails: f.santucci@unicampus.it, g.oliva@unicampus.it, r.setola@unicampus.it).

D. Lo Presti, and E. Schena are with the Unit of Measurements and Biomedical Instrumentation, Universitá Campus Bio-Medico di Roma, Rome, RM 00128 Italy. (e-mails: d.lopresti@unicampus.it, e.schena@unicampus.it)

The authors have no conflicts of interest to declare. All co-authors have seen and agree with the contents of the manuscript and there is no financial interest to report.

comparing the performance of wearable systems in different sensor positions in terms of measurement repeatability. Indeed, one of the major issues with wearable devices is that the signal waveform may change slightly depending on the subject and over repeated wearings of the same subject. Thus, an optimal sensor positioning should be identified also on the basis of a good measurement repeatability: the best sensor position should allow obtaining the most similar waveform for different subjects and even for repeated wearings of the same subject. Furthermore, for what concerns SCG signals collected using FBG-based wearables, the state of the art is focused on the HR estimation alone. Indeed, this technology is far less mature than magneto-inertial units to be used for SCG recording.

In this paper, we propose the use of a graph theory approach to evaluate the most promising position for SCG recording on the basis of the similarity among signals collected from two different positions on the chest: mitral valve and aortic valve auscultation site. We use graph mining to compare signals on the basis of the similarity among their waveforms. In other words, the proposed algorithm extracts a graph from each signal, compares the graphs belonging to the same group of signals and returns a *Group Similarity Score (GSS)* for the signals collected in the two sensor positions. The higher the *GSS*, the better the agreement among its members and the repeatability of the measure. Indeed, guaranteeing a good measurement repeatability means finding the sensor position that ensures to obtain the most similar waveform over multiple measurements. The proposed algorithm was tested on SCG signals collected simultaneously from the two sensor positions using two custom made wearable patches based on FBGs. Subsequently, the influence of the subject's posture on SCG waveforms was evaluated to find the optimal protocol for future ambulatory use.

HR values were also extracted by the captured SCG signals and compared to the reference ECG considering both the two measuring sites and different body postures to evaluate the ability of the wearable system to accurately detect physiological information and compare sensor performance in the two measurement sites. Our graph-theoretical methodology was designed to tackle two important open challenges in the field of wearable seismocardiography: *i)* optimizing sensor positioning for SCG recording from the chest based on the SCG waveform similarity and repeatability of the measure; *ii)* make a step forward in the validation of wearable systems based on FBG sensors for SCG recording.

The outline of the paper is as follows: in Section *Model and Analysis Framework* we introduce the graph-theoretical methodology we propose to compare SCG waveforms, in Section *Experimental Study* we illustrate the experimental trials performed, in Section *Sensor Positioning and waveform similarity Analysis using Graph Theory Approach* we explain the implementation of the proposed methodology on the collected data and the results obtained from the comparison analyses. To support the conclusions drawn, in Section *Sensor Positioning and Physiological Information using HR Analysis* we illustrate HR estimation from SCG recordings and the results obtained from the comparison analysis with the reference instrument (i.e., ECG). Finally, in Section *Comparison with accelerometer-based SCG measurement system* we compare the performance of the novel FBG-based wearable patches with the one of accelerometer-based systems which are considered the gold standard in this field.

II. Model and Analysis Frameworks

A. Graph Mining background

In this subsection, we briefly present the background of *graph mining*. The proposed graph theory approach will be discussed in detail in the following subsection. A graph is by definition a set of nodes, which can be connected by edges in pairs. Data mining aims at discovering interesting and/or useful patterns that are hidden in a given set of data. This innovative approach allows retrieving information on a dataset by processing the graph structures that can extracted from it. Such a novel method finds application in various and diverse scientific fields, such as bioinformatics, chemoinformatics, and computer/social networks. Different data mining approaches can be used for mining the graph-based data and performing useful analyses on these mined data. [13], [14], [15]

To the best of our knowledge, graph mining has been applied to seismocardiography only once in the literature. Indeed, Inan et al. devised a method to compare the structure of graphs derived from SCG signals collected after exercise and at rest in both compensated and decompensated heart failure (HF) patients [16]. In particular, in [16] the authors assessed the patients' state on the basis of a custom defined graph *similarity score* based on the number of links present in the graphs corresponding to two different signals. Moreover, they noted a significant change in graph *similarity score* from admission (decompensated) to discharge (compensated). These promising results revealed that graph mining is a sensitive enough methodology to compare SCG waveforms in order to assess their similarity.

Here, we propose a different graph-theoretical approach based on the construction of weighted graphs and on the computation of a fine-grained measure of graph similarity. This measure is based on a graph-theoretical analogue of the *energy* associated to an ensemble of particles. In particular, our approach differs from [16] in that we aim to construct a *similarity score* that provides a more granular information on the difference between two vectors of features. In fact, in our approach the weights correspond to the absolute value of the difference of the two endpoint features. Moreover, rather than counting the number of edges that are present in both graphs as in [16] (a measure that, thus, follows an on/off perspective) we provide a more nuanced and quantitative index based on the complete spectrum of the adjacency matrix of the *intersection graph*, in which each edge is weighted by the minimum of the weights of the edges in the two original graphs.

B. Proposed graph theory approach

Let $G = \{V, E, W\}$ be a *weighted graph* with n nodes $V = \{v_1, v_2, \ldots, v_n\}$, e edges $E \subseteq V \times V$, where $(v_i, v_j) \in E$ captures the existence of a link from node v_i to node v_j and

weights encoded by the $n \times n$ matrix W, where

$$W_{ij} = \begin{cases} w_{ij}, & \text{if } (v_j, v_i) \in E, \\ 0, & \text{otherwise,} \end{cases}$$

$w_{ij} \in \mathbb{R}$ being the weight associated to the link (v_i, v_j).

A graph is said to be *undirected* if the existence of an edge $(v_i, v_j) \in E$ implies the presence of $(v_j, v_i) \in E$, while it is said to be *directed* otherwise. In the following, we consider just undirected graphs. For undirected graphs we assume $w_{ij} = w_{ji}$, i.e., the weight matrix W is symmetric. An undirected graph is *connected* if each node can be reached by each other node via the edges in E. In the following, we consider graphs that are not necessarily connected. Let the neighborhood of a node v_i be the set of nodes v_j such that $(v_i, v_j) \in E$.

Given a weighted graph $G = \{V, E, W\}$, the associated *energy* [17] is defined as the sum of the absolute values of the eigenvalues of the weight matrix W, i.e.,

$$\sigma(G) = \sum_{i=1}^{n} |\mathtt{eig}_i(W)|,$$

where $\mathtt{eig}_i(W)$ is the eigenvalue of W with i-th largest magnitude.

Let us now consider weighted graphs $G_1 = \{V, E_1, W_1\}$ and $G_2 = \{V, E_2, W_2\}$ and let us define the *intersection graph* $G_1 \cap G_2$ as the graph over the same set V of nodes with edges that are the intersection of the two edge sets E_1 and E_2 and with weights that are the minimum of the weights over the two graphs, i.e.,

$$G_1 \cap G_2 = \{V, E_1 \cap E_2, \min\{W_1, W_2\}\},$$

where $\min\{W_1, W_2\}$ is the entrywise minimum of the two matrices W_1 and W_2.

In the following we use the energy

$$\sigma(G_1 \cap G_2) = \sum_{i=1}^{n} |\mathtt{eig}_i(\min\{W_1, W_2\})|,$$

as a measure of similarity between the graphs G_1 and G_2, i.e., the larger is $\sigma(G_1 \cap G_2)$ the more G_1 and G_2 are similar, while $\sigma(G_1 \cap G_2) = 0$ when the edge sets E_1, E_2 are disjoint, i.e., when $E_1 \cap E_2 = \emptyset$.

C. Proposed measure of similarity

Let $\boldsymbol{x} \in \mathbb{R}^n$ denote a vector and let us construct a graph G_x via the k-nearest neighbor technique. In other words, let us associate a node $v_i \in V$ to each component i of the vector $\boldsymbol{x}$ and let us create a link (v_i, v_j) connecting each node v_i with the k nodes having closest values of x_i. In particular, we assume the weight w_{ij} associated to a link (v_i, v_j) is $|x_i - x_j|$. As a result, we obtain a weighted graph $G_x = \{V, E_x, W_x\}$.

At this point, let us consider $\boldsymbol{x}, \boldsymbol{y} \in \mathbb{R}^n$ and let $G_x = \{V, E_x, W_x\}$ and $G_y = \{V, E_y, W_y\}$ denote the two graphs obtained via the k-nearest neighbor approach.

We evaluate the similarity of $\boldsymbol{x}$ and $\boldsymbol{y}$ in terms of the similarity of G_x and G_y, i.e., we assume $\sigma(G_x \cap G_y)$ represents a measure of similarity of $\boldsymbol{x}$ and $\boldsymbol{y}$.

III. Experimental study

A. Wearable system working principle

The wearable system used in the experimental study consists of two biopatches, each one integrating an FBG sensor. The FBG sensor is essentially a grating inscribed in a narrow segment of an optical fiber whose elements are stretches of fiber with an altered refractive index. Such a grating results from the exposure of the fiber core to a periodic pattern of intense laser light and leads to a fixed index modulation with a periodic variation along the propagation axis of the core. Hence, when a broad spectrum of wavelengths is passed through the FBG, its grating acts as a wavelength-specific dielectric mirror that back reflects a narrow bandwidth of wavelengths ad transmits all the others. The central wavelength of the reflected component is referred to as the Bragg wavelength, λ_B, and satisfies the Bragg condition [18], [19]:

$$\lambda_B = 2\eta_{eff}\Lambda,$$

where η_{eff} is the refractive index and Λ is the period of the refractive index variation in the grating. Due to the temperature and strain dependence of the parameters n and Λ, the wavelength of the reflected component changes also as a function of temperature change (ΔT) and/or applied strain (ϵ). This dependency allows determining the temperature or strain change from the shift in the reflected wavelength, which is given by:

$$\frac{\Delta\lambda_B}{\lambda_B} = \Delta T k_T + \epsilon k_\epsilon,$$

where the first term expresses the temperature effect on the fiber while the second term expresses the strain effect on the grating. Indeed, the coefficient k_T is determined by the thermal expansion and thermal-optic coefficients of the fiber, while the coefficient k_σ is determined by the physical elongation of the grating pitch and strain-optic coefficient of the fiber:

$$\frac{\Delta\lambda_B}{\lambda_B} = \Delta T(\alpha_\Lambda + \alpha_n) + \epsilon(1 - \rho_\epsilon),$$

with ρ_ϵ the strain optic coefficient, α_Λ the thermal expansion coefficient, and α_n the thermo-optic coefficient of the optical fiber. When FBGs are embedded within a coating matrix, the values of k_ϵ and k_T are different from the ones of the bare fiber, since they are affected by the mechanical and thermal properties of the material used to fabricate the external protective coating. However, the new values of k_ϵ and k_T can be easily determined by a sensor calibration process. In this application, FBGs undergo a strain of a few $\mu\epsilon$ causing a λ_B shift in the magnitude of pm. On the contrary, the temperature contribute can be considered negligible. The experimental sessions were performed at constant room temperature and the fiber grating was not in direct contact with the subjects' skin, but it was placed within a silicone-based matrix which was itself layered between two liners of kinesiological tape, which create a thermal insulation for the sensitive element. All these factors considered, the λ_B shift is given by the ϵ contribute only.

Each FBG sensor was encapsulated into a flexible matrix of silicone rubber, obtained by casting an appropriate amount of Dragon Skin^{TM} 20 (Smooth-On, USA) inside a 3D printed mould, previously designed in Solidworks. Silicones are certified as skin safe materials (ISO 10993-10), and they are highly suitable for use in sensors with biomedical applications due to their properties of elasticity and resistance to high temperatures.

The flexible matrix, embedding the FBG, was layered between two liners of kinesiological tape (Alpidex, Germany) to ensure a better mechanical coupling between the patch and the chest surface. The bottom layer, which gets in contact with the surface of the rib cage, shows a slit in correspondence of the sensing element in order to guarantee a direct contact between the sensitive part of the biopatch and the skin.

When the wearable patch is attached to the subject's chest, its volumetric expansions/contractions and microscopic deformations caused by the air inhalation/exhalation and pumping action of the heart, respectively, induce a strain on the patch surface, which leads to a shift in λ_B. More in detail, λ_B shifts to higher wavelength values in case of an expansion and to lower wavelength values in case of a compression of the patch and, consequently, of the embedded FBG. It must be considered that the perturbations caused by the heart beating are smaller than, and thus partially hidden by, the ones caused by the overlapping respiratory activity. Although this significant difference between the contribution of breathing-related and heart-related movement on the FBGs output, we have already demonstrated the possibility to perform a simultaneous monitoring of these two activities using FBG-based approach [20]. Moreover, the microscopic vibrations induced on the chest surface by the mechanical activity of the heart can be stressed in the absence of the respiratory contribution (for instance, working in the apnoea phase).

B. Wearable system design and fabrication

In this study, a wearable system consisting of 2 identical patches (each of dimensions $40mm \times 25mm \times 2mm$) was custom designed and fabricated. The system takes advantage of the multiplexing capability of FBGs, which allows them to be integrated in an array configuration for quasi-distributed measurements.

1) Wearable system design: The proposed solution amounts to a single optical fiber, housing two FBG sensors. In correspondence of the sensing elements of the fiber, two "dog-bone" shaped polymer housings of Dragon Skin^{TM} 20 were fabricated to confer a higher robustness to the sensory parts of the system and placed in between two fabric liners to guarantee a better adherence to the skin. This flexible casing makes the FBG easy to be stretched repetitive times without tearing and it rebounds to its original form without distortion. Dragon Skin^{TM} silicones are certified skin safe (ISO 10993-10) and due to their superior physical properties and flexibility are used in a variety of medical applications (e.g., prosthetic implants).

This configuration allows obtaining two simultaneous recordings of the SCG signal from two different locations on the chest via a single channel of the optical spectrum interrogator (see Figure 2.a). The individual elements of the wearable system are nominally identical to the one fabricated in [20], that we tested for respiratory and HR monitoring. Both the fabrication process and metrological characteristics of the single patch are described in more detail in [20].

2) Wearable system fabrication: In order to obtain the outer flexible shell, a mold was custom designed using a 3D CAD program (Solidworks) and 3D printed in polylacticacid (PLA) by Ultimaker 2 (Ultimaker, Utrecht, The Netherlands). The FBG sensor was placed at the centre of the 3D-printed mold before the polymer preparation and a pretension was applied to the extremities of the fiber to keep the cable tight. Then, Part A of the silicone was equally mixed with part B, and the mixture was degassed and poured into the mould in a single spot and with a uniform flow to minimize air entrapment while dispensing. Before demoulding, the rubber was let to cure at room temperature ($\sim$ 23 °C) for 4 h. During the fabrication process, the power spectrum of the pretensioned FBG sensor was collected before the silicone pouring and after vulcanization. No spectrum changes occurred in central wavelength (λ_B) and shape. Finally, two fabric liners were applied were applied to both sides of the flexible matrix obtained by the curing process. The fabric liners allow to enlarge the flexible matrix contact surface with the skin and facilitate the skin-sensor coupling.

3) Wearable-based measurement set-up: SCG signals were recorded from the volunteers by connecting the wearable system to an optical interrogator (si255 Hyperion Platform, Micron Optics Inc., Atlanta, GA, USA) at 1000 Hz. The interrogator functions as both a light source and a data acquisition system, since the content-rich output is the reflected wavelength. The measured data are sent to a laptop PC via cable connection. Data post-processing was executed in the MATLAB environment (MathWorks Inc., Natick, MA, USA).

C. Experimental protocol and setup

An experimental session on 11 healthy volunteers with no history of cardiorespiratory diseases was conducted to collect an adequate number of SCG signals in 2 positions for the waveform similarity analysis. The preclinical trial, entitled *Smart Textile - Università Campus Bio-Medico di Roma*, with protocol number ST-UCBM 27.2(18).20 OSS was granted by the Ethical Committee of the Università Campus Bio-Medico di Roma (Rome, Italy). In particular, 11 subjects (70 % males and 30 % females) were enrolled in the experimental study. The volunteers were all adults with an age of 28 $\pm$ 5 years old and a body mass index (BMI) of 24.2 $\pm$ 2.6 (both expressed as mean $\pm$ standard deviation). During the trials, the two wearable patches were attached in correspondence of two anatomical landmarks: the mitral valve (*xp*) and the aortic valve auscultation site (*av*) (Figure 1.a and 1.b). We chose the mitral valve because it is very near to the xiphoid process which is the most used position in the literature. Indeed, being the heart located in the middle of the sternum slightly moved to the left of the breastbone, this measurement site is the point at

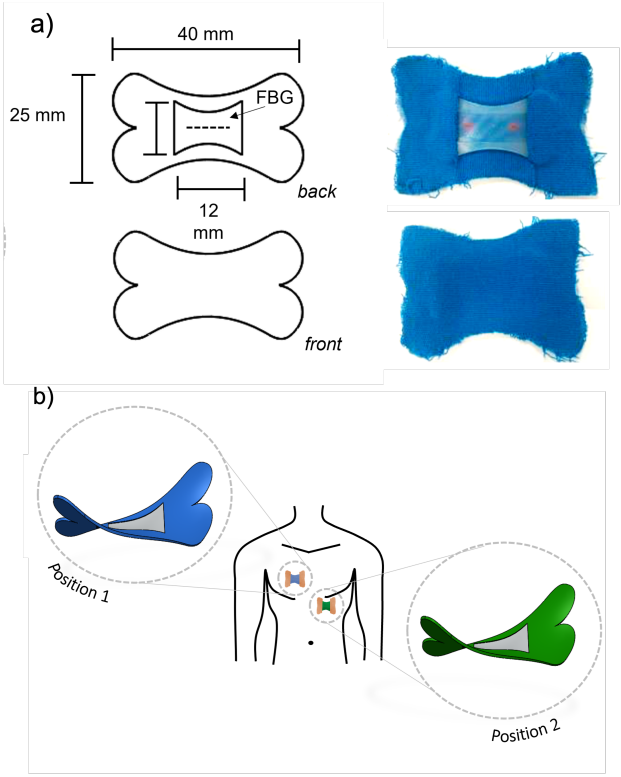

Fig. 1: a) Dimensions and picture of the sensor patch. b) Positions of the two wearable patches during SCG acquisition.

which vibrations are most intense [11]. As a counterpart for the comparison we chose the aortic valve auscultation site. The reason for this choice is that, according to the literature, this position has a number of interesting properties that make it a promising location for SCG measurement. Indeed, this is the area on the chest where the sounds of aortic valve opening (AO) and closure are loudest. This phenomenon is very important in SCG-related analyses, because the fiducial point corresponding to aortic valve opening on SCG signal is the reference point for HR extraction (i.e., the equivalent of R-peak for ECG signal) and for the estimation of important time intervals (e.g, Pre-ejection Pediod - PEP) [11], [21], [22], [23].

Each volunteer was invited to perform the following protocol: 30 s of apnoea at full lungs, a variable recovery phase of quiet breathing and 20 s of apnoea at empty lungs. Each volunteer was asked to repeat the same trial in three body postures: supine, sitting, and standing. Thus, at the end of the second stage of apnoea, each volunteer was invited to change the body position (the first time from laying down to sitting up and the second time from sitting to standing up) with a variable pause between the trials depending on the single subject need for resting time. During the testing procedure, ECG was collected as a reference using a commercially available chest strap (ZephyrTM performance systems, Medtronic, The Netherlands) at the sampling frequency of 250 Hz. Simultaneously, the outputs of the two wearable patches (i.e., the λ_B of the two FBGs which represent the SCG) were recorded using an optical spectrum interrogator (si255, Hyperon platform, LUNA Inc., Roanoke, VA, USA) at the sampling frequency of 1 kHz (see Figure 2).

D. Data set

For the analysis on the waveform similarity and optimization of the sensor position, the data collected in the experimental trials was organized in a private dataset. To only focus on the heart-related signal (i.e., the SCG), we decided to carry out the analysis on the signal parts collected during apnoea, where the breathing-related movements are absent.

The dataset includes 4 signals per volunteer in each posture: the signal relative to the apnoea phase with loaded lungs and the patch on *mv*, the signal relative to the apnoea phase with empty lungs and the patch on *mv*, the signal relative to the apnoea phase with loaded lungs and the patch on *av*, the signal relative to the apnoea phase with empty lungs and the patch on *av*. Considering that the volunteers enrolled were 11 and the postures assumed during the trials were 3 (i.e., lying, sitting and standing), the dataset contains in total 132 signals.

In order to remove the settling phase of the apnoea, corresponding to the initial peaks, raw data were pre-processed by cutting the signals from the thousandth sample onwards. Finally, all the signals were cut in order to have the same length, equal to the length of the shortest of the signals in the dataset. The final version of the signals is 14 s long.

IV. Sensor Positioning and Waveform Similarity Analysis Using Graph Theory Approach

The proposed approach based on graph mining was implemented on this private dataset to evaluate waveform similarity with respect to the position of the sensor (i.e., *mv*, and *av*). The aim was to assess whether the collected signals were more similar to each other when the sensor was positioned on *mv* or when the sensor was placed on *av*. A higher degree of similarity implies a higher repeatability of the measurement: if SCG signals are more similar to each other, it means that repeated fits of the same subject or different subjects with the sensor in that position result in more similar signals, all other conditions being equal. This translates into the guarantee of having a more similar waveform over multiple measurements by placing the sensor in a specific position.
A correct sensor positioning can be guaranteed and assisted by newly proposed algorithms for detecting and localizing SCG sensor misplacement [24], [25], [26], [27].

A. Implementation of the graph-theoretical approach

1) Inter-position analysis: The dataset was divided into 2 groups with respect to the sensor position (i.e., *mv*, and *av*). Each group contains 66 signals. For each vector $\boldsymbol{x} \in \mathbb{R}^n$ containing the signal samples, a graph G_x was computed via the k-nearest neighbor technique with the parameter k set to 1000. As in [16], to find the adequate value of k, results were computed for k=3, k=10, k=30, k=100, k=300, k=1000 and k=3000. Energy values appeared to grow with increasing k-value and with substantial difference in the final results. However, the increase in the GSS value comes at the

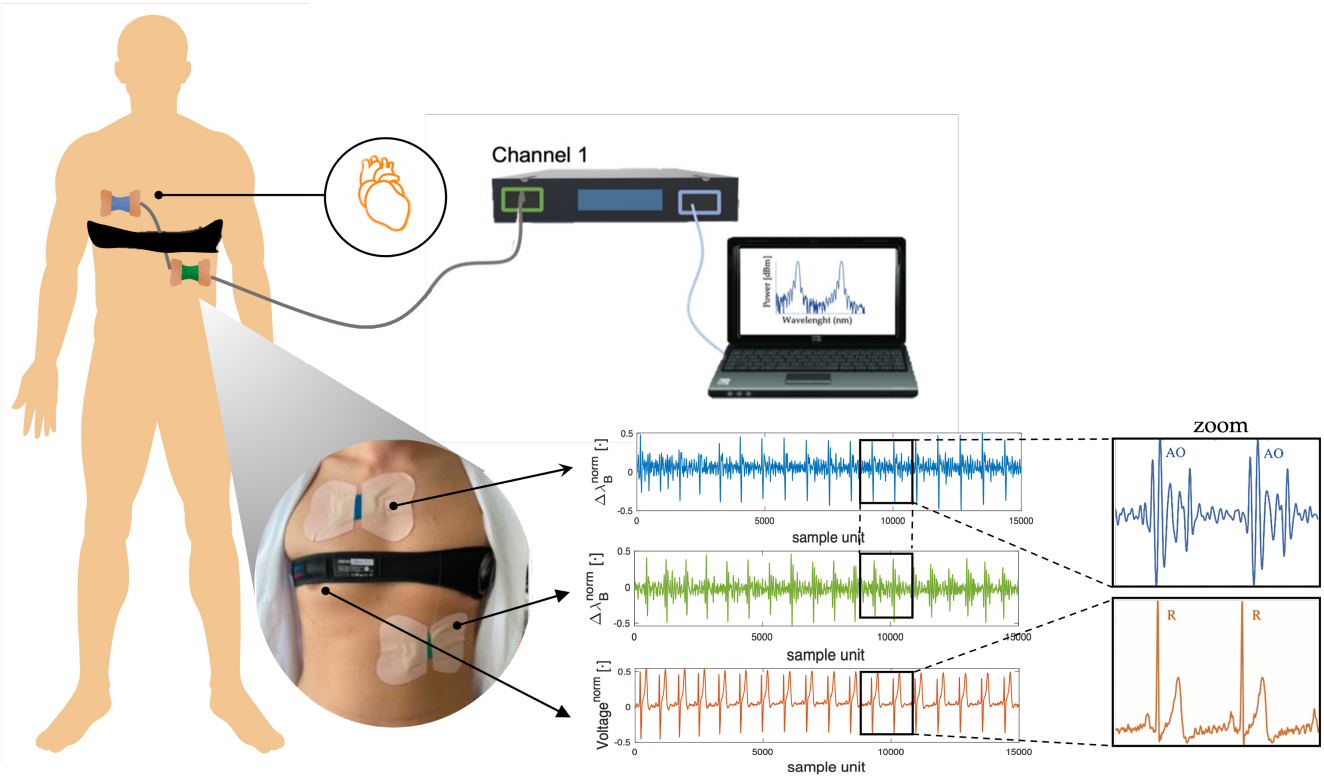

Fig. 2: Experimental setup and SCG signals collected during apnoea by means of two wearable patches from the mitral valve and aortic valve auscultation sites together with simultaneous ECG tracing.

expense of a greater computational cost and time (see Table I and Table II). For this reason we chose a value of k=300. In other words, a node $v_i \in V$ was associated to each sample value i of the signal vector $\boldsymbol{x} \in \mathbb{R}^n$. A link (v_i, v_j) was created to connect each node v_i with the k nodes having closest values of x_i. In this study, we assumed the weight w_{ij} associated to a link (v_i, v_j) as given by $|x_i - x_j|$. As a result, we obtained a weighted graph $G_x = \{V, E_x, W_x\}$ for each signal. At this point, let us consider x and $y \in \mathbb{R}^n$ which are two signals belonging to the same group and let $G_x = \{V, E_x, W_x\}$ and $G_y = \{V, E_y, W_y\}$ denote the two graphs corresponding to $\boldsymbol{x}$ and $\boldsymbol{y}$ respectively, obtained via the k-nearest neighbor approach. We evaluate the similarity of $\boldsymbol{x}$ and $\boldsymbol{y}$ in terms of the similarity of their graphs G_x and G_y, using as *similarity score* $\sigma(G_x \cap Gy)$ (see Figure 3). Thus, the energy of the intersection of the two graphs G_x and G_y is the measure of the similarity of the original signals that we wanted to compare (i.e., x and y). This process is reiterated for all the pairs of signals in each group taken once. At the end of the iteration, a *similarity score* is given for each of the two groups relative two the two sensor positions (mv and av), expressed as mean $\pm$ standard deviation. The proposed algorithm was implemented in Matlab environment that allows a semi-automated data processing.

2) Inter-posture analysis: The same analysis was performed on SCG signals collected on *av* and *mv*, divided into 3 groups depending on the subjects' posture. This analysis was addressed to detect changes in waveforms similarity with respect to the posture assumed by the subject. This investigation will show which posture returns most similar SCG waveforms for repeated measurements. This finding is particularly useful in order to theorize a protocol for an eventual medical examination to be included in the clinical practice.

TABLE I: Similarity scores (expressed as mean $\pm$ standard deviation) computed using raw data for sensor positions *mv* and *av* with respect to different values of k (3,10,30,100,300,1000,3000).

Similarity score		
k value (considering all postures)	*mv*	*av*
k=3	$1.9956 \times 10^{-4} \pm 9.0756 \times 10^{-4}$	$4.2066 \times 10^{-5} \pm 2.6570 \times 10^{-4}$
k=10	0.0070 ± 0.0203	0.0017 ± 0.0053
k=30	0.1198 ± 0.2259	0.0369 ± 0.0758
k=100	1.7578 ± 1.9797	0.5627 ± 0.7903
k=300	12.5174 ± 10.1060	4.3794 ± 4.3723
k=1000	70.4898 ± 47.3937	25.9990 ± 20.3499
k=3000	280.7313 ± 173.5818	99.1031 ± 65.5401

TABLE II: Simulation time and standard deviation for different values of k expressed in seconds and computed using two signals for each simulation test.

Simulation time for three pair of signals at different k values		
k value (considering all postures)	*mv*	*av*
mean and std k=3	781.92 ± 497.93	797.56 ± 505.07
mean and std k=10	909.90 ± 566.46	916.50 ± 589.52
mean and std k=30	1117.90 ± 704.05	1106.60 ± 691.35
mean and std k=100	1575.20 ± 12.46	1563.30 ± 3.84
mean and std k=300	1617.40 ± 19.70	1615.90 ± 22.29
mean and std k=1000	1618.50 ± 1.14	1635.6 ± 17.26
mean and std k=3000	1671.00 ± 22.96	1674.70 ± 23.28

At the end of this analyses, the optimal sensor position and posture of the subject for SCG measurement are given. The proposed algorithm was implemented in Matlab environment that allows a semi-automated data processing.

B. Statistical Analysis

The calculated mean values for the GSS between mv and av sensor positions were compared using Student's t-test. A significant difference was found between the groups in the GSS metric (i.e., 12.5174 ± 10.1060 for mv sensor position, while the result was 4.37945 ± 4.3723 for av sensor position, with significance value $p < 0.05$).

C. Results

1) Results of the inter-position analysis: The similarity score $\sigma(G_x \cap Gy)$ of SCG signals divided into 2 groups with respect to the sensor position (i.e., *mv* and *av*) revealed that SCG signals collected in *mv* position are more similar among each other than the ones collected on *av*. Indeed, the similarity score for *mv* position expressed as mean $\pm$ standard deviation is 12.5174 ± 10.1060, while the *similarity score* for av is 4.37945 ± 4.3723.

These findings provide evidence that support the conclusion that the mitral valve is the most promising sensor position based on the proposed similarity score against the aortic valve auscultation site. Thanks to the algorithm design, this means that by placing the sensor on several people in *mv* position, SCG signals obtained are more similar among each other than the ones obtained by placing the sensor in av. In view of a future clinical examination, taking the mitral valve as a reference for sensor positioning, both the inter- and intra-subject variability of the SCG signal could be reduced with respect to the aortic valve auscultation site.

In a way, these results confirm what can be found in the literature about the lower left sternum being a promising measuring point for SCG signal. However, in this study we demonstrated that at this specific location the repeatability of the signal waveform is good and better than another promising point (i.e., *av*). Therefore, in view of a clinical examination it would be appropriate to place the SCG sensor on *mv* because the signal has a high intra-subject repeatability and a low inter-subject variability.

2) Results of the inter-posture analysis: The similarity scores of SCG signals divided into 3 groups with respect to the subjects' posture (i.e., laying, standing and sitting), reported in Table III, revealed that SCG signals collected in *mv* position are more similar among each other when the subject is laying down. On the one hand, these findings confirm that the *mv* position is the best one in all 3 postures. On the other hand, they suggest that in *mv* position the highest *similarity score* is obtained in laying position.

Thus, in view of a clinical examination it would be appropriate to record the SCG signal with the sensor attached on *mv* while the subject is in laying position. These considerations ensure so far that the SCG waveform has the best intra-subject repeatability and the lowest inter-subject variability using this protocol.

TABLE III: Similarity scores (expressed as mean $\pm$ standard deviation) computed using raw data for sensor positions *mv* and *av* with respect to the subject's posture (i.e., laying, sitting, standing).

Similarity score		
Posture	mv	av
Laying	16.12 ± 14.08	4.08 ± 3.68
Sitting	12.69 ± 8.25	4.63 ± 4.75
Standing	9.31 ± 7.91	4.15 ± 3.82

V. Sensor Positioning and Physiological Information using HR Analysis

A. HR extraction

SCG and ECG raw data collected using the wearable system and Bioharness were synchronized. All signals were processed to preserve 14 s of trace as explained in more detail in Section *Dataset*. Traces relative to the apnoea at full lungs and apnoea at empty lungs were considered as separate signals until final error computation.

1) Signals pre-processing: SCG signals were extracted from raw data recorded by the wearable system using a first-order Butterworth bandpass filter (BPF) with lower cut-off frequency of 10 Hz and higher cut-off frequency of 30 Hz. ECG traces were pre-processed using a first-order Butterworth BPF with lower cut-off frequency of 5 Hz and higher cut-off frequency of 26 Hz.

2) PSD analysis: The estimation of HR by SCG signals was performed considering the peaks related to the aortic valve opening. This event was detected on the SCG envelope considering the output of each wearable patch. The reference HR values were estimated by identifying the R peaks of the ECG signal.

At first, the upper and lower envelopes of the input SCG were determined using the magnitude of its analytic signal computed using the discrete Hilbert Transform. Then, the lower envelope was filtered using a third-order Butterworth filter with lower cut-off frequency of 0.7 Hz and upper cut-off frequency of 2 Hz. The extraction of HR values from filtered SCG envelopes was performed in the frequency domain using PSD estimation.

Absolute ECG traces were filtered in the HR range using a first-order Butterworth BPF with lower cut-off frequency of 0.7 Hz and higher cut-off frequency of 2 Hz. PSD was computed for each signal and the dominant frequency of each spectrum was found as the frequency value at which the maximum peak of the spectrum occurs. On the basis of the PSD dominant frequency value, the number of beats per minute (bpm) is estimated for each signal.

B. Statistical analysis

The agreement between the HR values measured by the wearable system (i.e., HR_{SCG}) and those measured by the gold standard (i.e., HR_{ECG}) was evaluated in terms of percentage error (err). To estimate the err values for HR

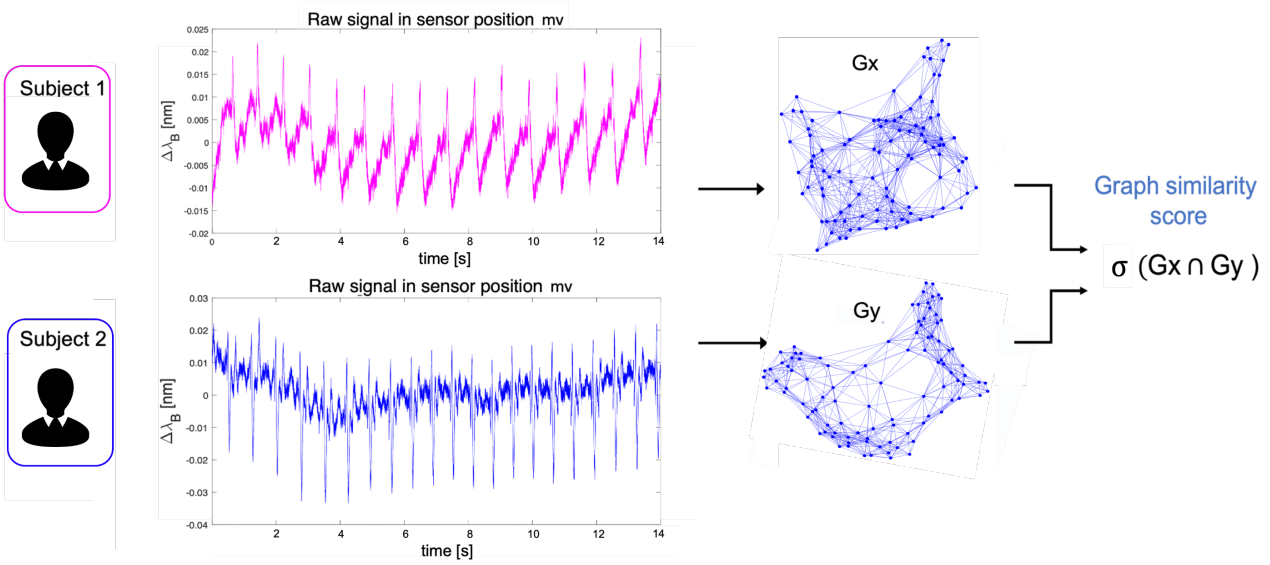

Fig. 3: Visual representation of the steps for computing the *similarity score*.

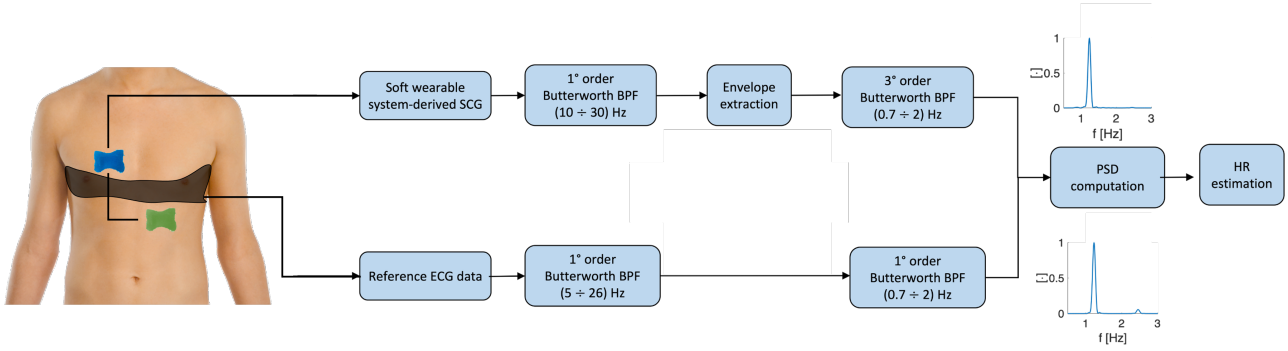

Fig. 4: Processing steps in HR analysis.

monitoring, the percentage error was computed as the ratio between the absolute error and the magnitude of the reference value percent:

$$err(\%) = \frac{(HR_{SCG} - HR_{ECG})}{HR_{ECG}} \times 100$$

An err value for each subject in each posture and sensor position was computed considering apnoea at full lungs and apnoea at empty lungs as separate traces. Then, a final err value for each subject by averaging the err value obtained in each sensor position during apnoea at full lungs and apnoea at empty lungs, considering each posture separately. Final errors are shown schematically in IV. Negative values express the FBG sensor tendency to underestimate the reference while positive values express the FBG sensor tendency to overestimate the reference.

C. Results

The overall trend of err values is very low, confirming the reliability of recorded SCG signals and thus the validity of the wearable system for an accurate measurement of HR. Results of err computation show that the lowest err values are obtained for the patch in *mv* position and with the subject in the laying posture (err values for subject 1, 2, 3, 4 and 9). For what concerns the subject's posture, lower err values are obtained in laying posture, followed by sitting posture and standing posture respectively.

For what concerns the measurement sites considered, it can be stated that the lower err values are obtained for *mv* measurement site. Mean error values show that the lowest errors are obtained in mv position in all laying (-0.0055 %), sitting (0.8609 %) and standing (-0.1273 %) postures.

These findings validate results obtained in the waveform similarity analysis, confirming that the best measurement site

for SCG recording is in correspondence of the mitral valve auscultation site and the best posture is lying down.

TABLE IV: final err values for each subject in each posture and sensor position.

Error values (%)						
Subject	**Laying posture**		**Sitting posture**		**Standing posture**	
	mv	**av**	**mv**	**av**	**mv**	**av**
s_1	-0.06	-0.06	0.3	-0.01	0.7	0.1
s_2	-0.05	-0.8	0.2	0.5	-0.2	0.5
s_3	0.07	0.2	-0.5	-0.7	-2.0	2.1
s_4	0.04	-0.3	0.1	0.2	-1.6	-3.5
s_5	-2.0	-2.3	-0.7	0.7	0.2	0.3
s_6	3.6	0.7	0.4	0.3	0.7	0.6
s_7	0.5	-0.03	11	43	0.7	3.9
s_8	-2.4	-2.4	-2.4	-2.4	0.5	-1.8
s_9	-0.04	-5	-0.4	0.3	-0.6	-0.3
s_{10}	-0.2	-0.2	-0.03	3.2	0.7	2.9
s_{11}	0.5	0.6	1.6	1.3	-0.5	-0.2
Mean error values (%)						
	-0.01	-0.87	0.86	4.2	-0.13	0.42

VI. Comparison with accelerometer-based SCG measurement system

To better investigate the capability of the proposed wearable patches based on FBG technology in monitoring SCG signal, we carried out an additional experimental test to compare the SCG retrieved by the FBG with the one obtained using an accelerometer (traditionally used as SCG benchmark).

A. Experimental protocol and setup

In order to compare the proposed FBG-based wearable to a more standard accelerometer-based SCG measurement system, we carried out an experimental session on a single subject employing both systems simultaneously. For this purpose, a male volunteer of age 24 and BMI of 23.2 was enrolled. Similarly to the previous experimental session, the male volunteer was asked to perform a protocol that sequentially included three postures: laying down, sitting, and standing. In each posture, the subject was asked to perform 2 apnoea phases of 30 seconds each, at loaded and empty lungs respectively. Despite the challenging demand, the subject managed to maintain 30 seconds of apnoea and therefore the signals considered were all 30 s long.

The accelerometer-based system assumed as a gold standard is a small ($36 \times 30 \times 11mm$) IMU sensor (Xsens DOT, by Xsens), embedding a tri-axial accelerometer (standard full range of $\pm 16g$ and sensitivity of 2048 LSB/g) and a tri-axial gyroscope (full scale $\pm 2000°/s$). Two Xsens DOT devices were fixed in correspondence of the two sensor positions considered (i.e., mv and av) just above the corresponding FBG-based wearable patch (see Figure 5). The Xsens DOT wearable is small in size and light in weight ($11.2g$), but the rigid housing containing the inertial sensors allows a worse adherence to the skin compared to the soft wearable patch. Moreover, the external housing makes the whole sensor larger than the "point" accelerometer it embeds, worsening the sensitivity of the bare sensor, just as in the case of the FBG sensor once it is encapsulated within a larger polymer matrix. Accelerometers data were collected at 60 Hz and saved in the internal memories of the devices. Although information content was present in all 3 axis, we chose to use the z-axis SCG signal as the most promising for this type of analysis [28], [7], [29]. The wearable Zephyr Bioharness TM device (Zephyr Technology Corporation, Annapolis, MD, USA) was used to record the simultaneous ECG waveform at 250 Hz and the respiratory waveform at 25 Hz. The respiratory signal was used to identify and cut out the apnoea parts on the other signals. FBG-derived signals were collected at a sampling frequency of 1 kHz. Before further processing, ECG and respiratory data were re-sampled at 100 Hz.

B. Comparison based on physiological information using HR analysis

All SCG and ECG signals were synchronized. All apnoea signals were 30 s long. Traces relative to the apnoea at full lungs and apnoea at empty lungs were considered as separate signals until final error computation. For HR extraction the same processing steps described in Section V and resumed in Figure 4 were adopted. The error committed in HR estimation with respect to the reference ECG was estimated in terms of percentage error for both SCG measurement systems in all apnoea phases. The final err values for each system in each subject posture and sensor position were computed by averaging the err values obtained during apnoea at full and empty lungs, considering each posture separately (see Table V). The small entity and similarity of errors committed by the FBG and accelerometer-based systems demonstrate the validity of the novel FBG-based wearable system for SCG measurement as well as its high sensitivity, which is only minimally affected by encapsulation in a polymer matrix.

VII. Limitations

The illustrated graph-theoretical approach was proposed to tackle a fundamental open challenge in the field of wearable seismocardiography: optimizing sensor positioning for SCG recording from the chest. This methodology aims at finding the best sensor position based on the SCG waveform similarity and repeatability of the measure. In the literature, very few attempts have been made to assess the optimal position on the chest for SCG recording [11], [12], [30] and none of these has focused on waveform similarity. The literature is lacking in definitive studies comparing the performance of wearable systems in different sensor positions in terms of measurement repeatability. In our experimental study we considered the two measurement sites that seem to be the most promising sensor positions for SCG recording. A limiting factor of this study could be that we only considered the two most promising positions.

The proposed methodology was tested on 11 healthy volunteers with age of 28 ± 5 years old and a BMI of 24.2 ± 2.6 (expressed as mean $\pm$ standard deviation), were enrolled. The population sample comprises both female and male subjects. A lower BMI would likely allow a better adherence of the sensor to the point of interest on the chest, leading to a cleaner

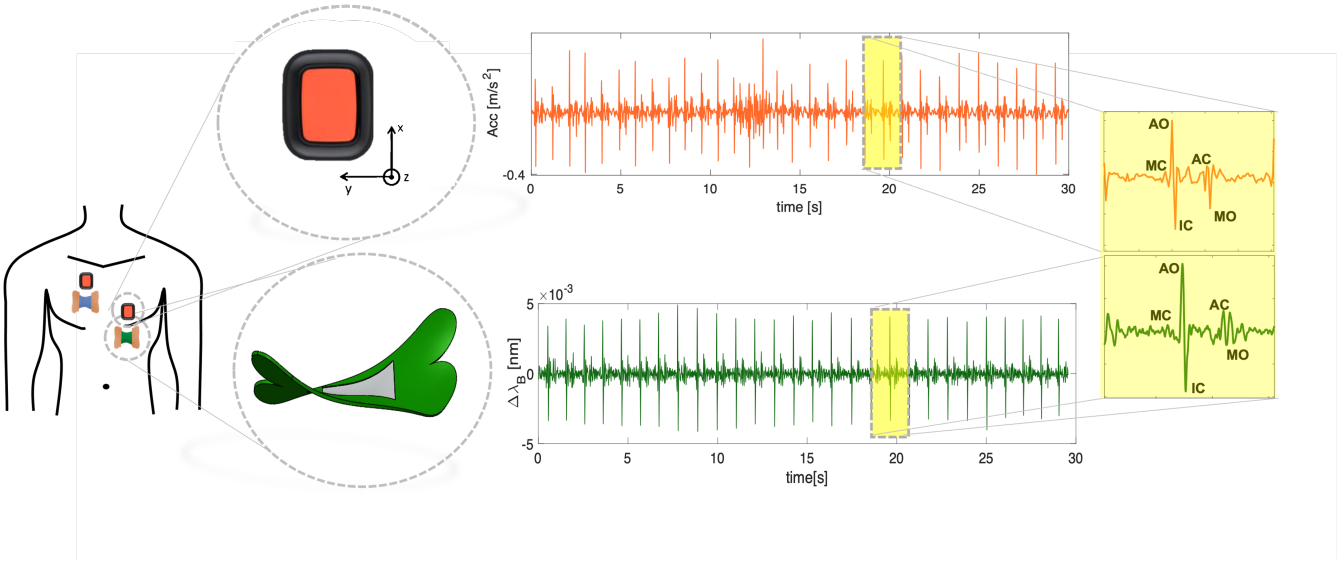

Fig. 5: Experimental setup for the comparison analysis.

TABLE V: final err values for the FBG-based and accelerometer-based SCG measurement systems in each posture and sensor position.

Error values (%)											
Laying posture				Sitting posture				Standing posture			
FBG-based wearable		Accelerometer-based system		FBG-based wearable		Accelerometer-based system		FBG-based wearable		Accelerometer-based system	
mv	av	mv	av	mv	av	mv	av	mv	av	mv	av
-1.15	-1.00	-0.01	-1.58	-3.16	-3.23	-0.15	1.88	7.23	7.26	-6.31	-0.33

SCG signal. For instance, in children, the SCG morphology is similar to that of adults with comparable amplitude for the mitral opening (MO) feature, higher amplitudes for other features and a little shortening in time parameters [31].

Subjects with a high BMI (i.e., obese people, BMI: 30 - 34.9 kg/m2) represent a more critical issue when it comes to SCG recording. However, Inan et al. [5] proved that graph mining is a sensitive enough methodology to compare SCG waveforms in order to assess their similarity even on people bordering on obesity. In this view, further developments of our study could be devoted to the application of the proposed method on subjects with very different BMIs.

Although the proposed methodology helped in providing the optimal sensor position for a reproducible SCG recording, a correct sensor positioning on the subject's chest by the clinician must be ensured in order to obtain a clean SCG signal. However, in this regard, a few algorithms for detecting and localizing SCG sensor misplacement have been proposed recently [24], [25], [26], [27]. For instance, Ashouri et al. devised a method to automatically detect when the sensor is placed in any position other than the desired one based on the fact that the regression curve for estimating PEP from SCG signals differs significantly as the position of the sensor changes [24]. Alternatively, Etemadi et al. in [26] proposed the use of a machine learning (ML) algorithm to detect sensor misplacement. Multiple features were extracted from SCG signals measured on healthy subjects in 5 different chest positions representing locations at which a user may accidentally misplace the hardware. Instances were labeled as correct position (midsternal position) and incorrect positions (4 other locations). A boosted J48 decision tree classifier with an Adaptive Boosting algorithm was then trained to automatically determine sensor misplacement on the basis of signal changes associated with sensor location. An overall precision of 0.83 and recall of 0.82 were achieved with this classifier. This performance was estimated sufficient to reduce the error in PEP estimation by 10 ms in unsupervised settings.

Additionally, using ML techniques, Zia et al. managed to detect and localize SCG sensor misplacement with ensembled quadratic discriminant classifiers [27]. In view of this, a correct sensor positioning can be guaranteed and assisted by newly proposed algorithms for sensor misplacement.

VIII. Conclusion

We used graph mining to evaluate the most promising position for SCG recording on the basis of waveform similarity among signals collected from two sensor positions: *mv* and *av*.

For each signal a graph was computed via the k-nearest neighbor technique: a node was associated to each sample and a weighted link was created to connect the pair of closest nodes. Graphs were used to compare signals belonging to the same group. The energy of the intersection of two graphs was used as a measure of the similarity between signals. This process was iterated for all the pairs of signals in each group. A *GSS* expresses the repeatability of the measurement in each position. The same analysis was performed on signals with respect to posture. Results demonstrated that the higher measurement repeatability is obtained with the sensor on *mv* and the subject laying down. These results were confirmed by the physiological information analysis and are independent of

the system used: a comparison analysis was carried out on a single subject using FBGs and accelerometers simultaneously. The accelerometer is smaller and lighter, but its rigid housing impacts the sensitivity of the bare sensor and its adherence to the skin.
HR analysis returned err values broadly similar for both systems.

These findings are a step forward in the optimization of sensor positioning in wearable seismocardiography and can be exploited to design more efficient protocols. These conditions appear applicable in clinics: the mv is a well-identifiable anatomical landmark that facilitates sensor positioning, and the laying position is comfortable during medical examinations.

Future studies may be devoted to applying the methodology to real patients' data. Being this algorithm designed to elaborate raw data, it could be implemented on signals from HF patients for identifying cardiovascular dysfunctions on the basis of SCG tracings.

REFERENCES

[1] K. Tavakolian, "Characterization and analysis of seismocardiogram for estimation of hemodynamic parameters," Ph.D. dissertation, Applied Science: School of Engineering Science, 2010.

[2] K. Tavakolian, A. P. Blaber, B. Ngai, and B. Kaminska, "Estimation of hemodynamic parameters from seismocardiogram," in *2010 Computing in Cardiology*. IEEE, 2010, pp. 1055–1058.

[3] M. M. H. Shandhi, J. Fan, J. Heller, M. Etemadi, L. Klein, and O. Inan, "Estimation of changes in intracardiac hemodynamics using wearable seismocardiography and machine learning in patients with heart failure: a feasibility study," *IEEE Transactions on Biomedical Engineering*, 2022.

[4] H. Sato, A. Ogawa, A. Takahashi, S. Fujiwara, Y. Sakurai, T. Kayama, and T. Yoshimoto, "Influence of superior cervical ganglion on cerebral hemodynamics–measurements of cerebral blood flow and metabolism during superior cervical ganglionectomy in patients with moyamoya disease," *No to Shinkei= Brain and Nerve*, vol. 42, no. 2, pp. 203–208, 1990.

[5] N. Zavanelli, H. Kim, J. Kim, R. Herbert, M. Mahmood, Y.-S. Kim, S. Kwon, N. B. Bolus, F. B. Torstrick, C. S. Lee *et al.*, "At-home wireless monitoring of acute hemodynamic disturbances to detect sleep apnea and sleep stages via a soft sternal patch," *Science advances*, vol. 7, no. 52, p. eabl4146, 2021.

[6] E. M. Johnson, J. A. Heller, F. Garcia Vicente, R. Sarnari, D. Gordon, P. M. McCarthy, A. J. Barker, M. Etemadi, and M. Markl, "Detecting aortic valve-induced abnormal flow with seismocardiography and cardiac mri," *Annals of biomedical engineering*, vol. 48, no. 6, pp. 1779–1792, 2020.

[7] O. T. Inan, P.-F. Migeotte, K.-S. Park, M. Etemadi, K. Tavakolian, R. Casanella, J. Zanetti, J. Tank, I. Funtova, G. K. Prisk *et al.*, "Ballistocardiography and seismocardiography: A review of recent advances," *IEEE journal of biomedical and health informatics*, vol. 19, no. 4, pp. 1414–1427, 2014.

[8] D. Rai, H. K. Thakkar, S. S. Rajput, J. Santamaria, C. Bhatt, and F. Roca, "A comprehensive review on seismocardiogram: current advancements on acquisition, annotation, and applications," *Mathematics*, vol. 9, no. 18, p. 2243, 2021.

[9] A. Taebi, B. E. Solar, A. J. Bomar, R. H. Sandler, and H. A. Mansy, "Recent advances in seismocardiography," *Vibration*, vol. 2, no. 1, pp. 64–86, 2019.

[10] F. Santucci, D. Lo Presti, C. Massaroni, E. Schena, and R. Setola, "Precordial vibrations: A review of wearable systems, signal processing techniques, and main applications," *Sensors*, vol. 22, no. 15, 2022. [Online]. Available: https://www.mdpi.com/1424-8220/22/15/5805

[11] R. H. Sandler, M. K. Azad, J. D'Angelo, P. Gamage, N. Y. Raval, R. J. Mentz, and H. A. Mansy, "Documenting spatial variation of scg signals for optimal sensor placement," *Journal of Cardiac Failure*, vol. 26, no. 10, p. S92, 2020.

[12] D. Lo Presti, F. Santucci, C. Massaroni, D. Formica, R. Setola, and E. Schena, "A multi-point heart rate monitoring using a soft wearable system based on fiber optic technology," *Scientific reports*, vol. 11, no. 1, pp. 1–10, 2021.

[13] S. Aridhi and E. M. Nguifo, "Big graph mining: Frameworks and techniques," *Big Data Research*, vol. 6, pp. 1–10, 2016.

[14] A. Inokuchi, T. Washio, and H. Motoda, "Complete mining of frequent patterns from graphs: Mining graph data," *Machine Learning*, vol. 50, no. 3, pp. 321–354, 2003.

[15] S. U. Rehman, A. U. Khan, and S. Fong, "Graph mining: A survey of graph mining techniques," in *Seventh International Conference on Digital Information Management (ICDIM 2012)*. IEEE, 2012, pp. 88–92.

[16] O. T. Inan, M. Baran Pouyan, A. Q. Javaid, S. Dowling, M. Etemadi, A. Dorier, J. A. Heller, A. O. Bicen, S. Roy, T. De Marco *et al.*, "Novel wearable seismocardiography and machine learning algorithms can assess clinical status of heart failure patients," *Circulation: Heart Failure*, vol. 11, no. 1, p. e004313, 2018.

[17] G. Ivan, "The energy of a graph," *Ber Math Statist Sekt Forschungsz Graz*, vol. 103, pp. 1–22, 1978.

[18] T. Erdogan, V. Mizrahi, P. Lemaire, and D. Monroe, "Decay of ultraviolet-induced fiber bragg gratings," *Journal of applied physics*, vol. 76, no. 1, pp. 73–80, 1994.

[19] D. Presti, C. Massaroni, C. Leitão, F. Domingues, M. Sypabekova, D. Barrera, I. Floris, L. Massari, C. Oddo, I. Iordachita, D. Tosi, and E. Schena, "Fiber bragg gratings for medical applications and future challenges: A review," *IEEE Access*, vol. PP, pp. 1–1, 08 2020.

[20] D. Lo Presti, D. Bianchi, C. Massaroni, A. Gizzi, and E. Schena, "A soft and skin-interfaced smart patch based on fiber optics for cardiorespiratory monitoring," *Biosensors*, vol. 12, no. 6, p. 363, 2022.

[21] T. Choudhary, M. Bhuyan, and L. Sharma, "A novel method for aortic valve opening phase detection using scg signal," *IEEE Sensors Journal*, vol. 20, no. 2, pp. 899–908, 2019.

[22] T. Choudhary, L. Sharma, and M. K. Bhuyan, "Automatic detection of aortic valve opening using seismocardiography in healthy individuals," *IEEE journal of biomedical and health informatics*, vol. 23, no. 3, pp. 1032–1040, 2018.

[23] J. Centracchio, E. Andreozzi, D. Esposito, G. D. Gargiulo, and P. Bifulco, "Detection of aortic valve opening and estimation of pre-ejection period in forcecardiography recordings," *Bioengineering*, vol. 9, no. 3, p. 89, 2022.

[24] H. Ashouri and O. T. Inan, "Automatic detection of seismocardiogram sensor misplacement for robust pre-ejection period estimation in unsupervised settings," *IEEE sensors journal*, vol. 17, no. 12, pp. 3805–3813, 2017.

[25] H. Ashouri, S. Hersek, and O. T. Inan, "Universal pre-ejection period estimation using seismocardiography: Quantifying the effects of sensor placement and regression algorithms," *IEEE sensors journal*, vol. 18, no. 4, pp. 1665–1674, 2017.

[26] M. Etemadi and O. T. Inan, "Wearable ballistocardiogram and seismocardiogram systems for health and performance," *Journal of Applied Physiology*, vol. 124, no. 2, pp. 452–461, 2018.

[27] J. Zia, J. Kimball, S. Hersek, M. M. H. Shandhi, B. Semiz, and O. T. Inan, "A unified framework for quality indexing and classification of seismocardiogram signals," *IEEE journal of biomedical and health informatics*, vol. 24, no. 4, pp. 1080–1092, 2019.

[28] M. J. Tadi, O. Lahdenoja, T. Humanen, J. Koskinen, M. Pänkaälä, and T. Koivisto, "Automatic identification of signal quality for heart beat detection in cardiac mems signals," in *2017 IEEE EMBS International Conference on Biomedical & Health Informatics (BHI)*. IEEE, 2017, pp. 137–140.

[29] M. Kaisti, M. J. Tadi, O. Lahdenoja, T. Hurnanen, A. Saraste, M. Pänkäälä, and T. Koivisto, "Stand-alone heartbeat detection in multidimensional mechanocardiograms," *IEEE Sensors Journal*, vol. 19, no. 1, pp. 234–242, 2019.

[30] R. Fadil, P. Aarotale, B. Hoffmann, F. Khosrow-Khavar, Z. G. Xiao, A. Akhbardeh, and K. Tavakolian, "Temporal changes of fiducial seismocardiogram points due to different sensor placements on the chest," in *2020 Computing in Cardiology*. IEEE, 2020, pp. 1–4.

[31] N. Jähne-Raden, H. Gütschleg, M. C. Wolf, S. Sigg, and U. Kulau, "Seismocardiography on infants and kids," in *2020 Computing in Cardiology*. IEEE, 2020, pp. 1–4.